

# STADI: Fine-Grained Step-Patch Diffusion Parallelism for Heterogeneous GPUs

Han Liang\*, Jiahui Zhou\*, Zicheng Zhou\*, Xiaoxi Zhang\*<sup>†</sup>, Xu Chen\*<sup>†</sup>

\*Sun Yat-sen University

Email: \*{liangh68, zhoujh77, zhouzch7}@mail2.sysu.edu.cn,

\*{zhangxx89, chenxu35}@mail.sysu.edu.cn

**Abstract**—The escalating adoption of diffusion models for applications such as image generation demands efficient parallel inference techniques to manage their substantial computational cost. However, existing diffusion parallelism inference schemes often underutilize resources in heterogeneous multi-GPU environments, where varying hardware capabilities or background tasks cause workload imbalance. This paper introduces Spatio-Temporal Adaptive Diffusion Inference (STADI), a novel framework to accelerate diffusion model inference in such settings. At its core is a hybrid scheduler that orchestrates fine-grained parallelism across both temporal and spatial dimensions. Temporally, STADI introduces a novel computation-aware step allocator applied after warmup phases, using a least-common-multiple-minimizing quantization technique to reduce denoising steps on slower GPUs and execution synchronization. To further minimize GPU idle periods, STADI executes an elastic patch parallelism mechanism that allocates variably sized image patches to GPUs according to their computational capability, ensuring balanced workload distribution through a complementary spatial mechanism. Extensive experiments on both load-imbalanced and heterogeneous multi-GPU clusters validate STADI’s efficacy, demonstrating improved load balancing and mitigation of performance bottlenecks. Compared to patch parallelism, a state-of-the-art diffusion inference framework, our method significantly reduces end-to-end inference latency by up to 45% and significantly improves resource utilization on heterogeneous GPUs.

**Index Terms**—Diffusion Model Inference, heterogeneous multi-GPU systems, parallelism strategies

## I. INTRODUCTION

Diffusion models, which were first proposed by [1], have emerged as a dominant force in generative artificial intelligence, sparking explosive growth across diverse applications. From generating photorealistic images [2]–[4] and videos [5]–[7] to revolutionizing text-to-speech synthesis [8], [9], and multimodal content creation [10], [11], these models demonstrate unparalleled capabilities in synthesizing high-fidelity outputs from complex data distributions. However, as deployment shifts from research prototypes to real-world systems, the substantial computational demands and inherent iterative nature of diffusion sampling present a significant challenge: *prohibitive end-to-end inference latency*. This bottleneck not only hinders user experience in interactive applications but also limits the feasibility of deploying these powerful models on resource-constrained devices or in time-sensitive scenarios.

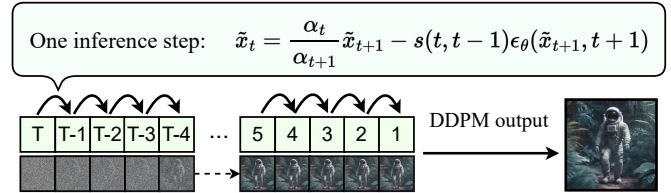


Fig. 1. DDPM inference illustration.

As illustrated in Figure 1, diffusion model inference (e.g., DDPM [1]) is a denoising process consisting of a sequence of *steps* for each request, indexed as  $T \rightarrow \dots t + 1, t \rightarrow \dots 0$ . In each step  $t$ , a trained neural network predicts the noise  $\epsilon_\theta(x_t, t)$ , based on the output (a noisy sample  $x_{t+1}$ ) of step  $t + 1$ , and a scaled version of  $\epsilon_\theta(x_t, t)$  is subtracted from  $x_{t+1}$ , to predict  $x_t$ . This process progressively recovers the target data distribution from the pure noise. The core bottleneck manifests as two interrelated factors: (1) the time per denoising step, and (2) the total number of required steps. For the former, its duration is primarily constrained by the computational complexity of the model’s forward propagation, which is often dominated by U-Net architectures [1]–[3] or transformer blocks [4]. Strategies have centered on model compression techniques and GPU-level optimizations. Reducing the number of required sampling steps is equally critical. e.g., DDPM [1] often necessitates thousands of steps for convergence.

**Advanced parallelism for diffusion inference.** To fundamentally decouple sampling latency from iterative step constraints, multi-GPU parallel inference paradigms [12]–[17] have emerged as a transformative approach. Key innovations in this area include: DistriFusion [12], which proposes *patch parallelism* with asynchronous stale activation reuse to achieve near-linear speedup; PipeFusion [13], deploying a chunked pipeline strategy that slices transformer layers and then also leverages patch parallelism to optimize memory scaling for high-resolution DiT-based models; and AsyncDiff [14], which divides the model into several blocks with roughly equal computational complexity and assigns them to multiple GPUs for pipeline parallel execution. Although these methods achieve near-linear speedups in homogeneous clusters with dedicated resources, their efficacy sharply degrades in systems with heterogeneous GPU speeds. As depicted in Figure 2, such

<sup>†</sup>Corresponding author: Xiaoxi Zhang, Xu Chen.

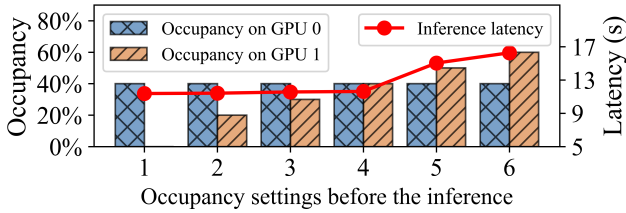


Fig. 2. The end-to-end inference latency of patch parallelism is constrained by the device with the lowest available computing power, (i.e., the highest occupancy). “Occupancy” represents the percentage of GPU consumed by background tasks.

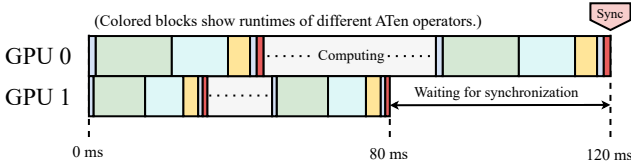


Fig. 3. Illustration of a single step of patch parallelism [12] inference distributed across 2 GPUs, each of which processes a equal portion (1/2) of the image. Due to heterogeneous computational capabilities or background workload imbalances, the faster GPU must wait for the slower one to complete synchronization at the end of the step.

heterogeneity, caused by hardware differences or imbalanced task occupancies across GPUs, increases inference latency and undermines resource utilization. Figure 3 further shows how this computational imbalance across devices cascades into blocking bottlenecks via inevitable per-step synchronization. These limitations underscore the necessity of adaptive frameworks robust to heterogeneity in both hardware and workloads.

**Existing multi-GPU methods for non-diffusion inference** consist of two main categories. One focuses on system-level scheduling for multi-task workloads for throughput maximization [18]–[21], neglecting intra-request acceleration. The other targets single-task inference via three main parallelism strategies: pipeline parallelism, which partitions the model into layers assigned to different GPUs [22]–[24]; tensor parallelism [25], which splits weight matrices within layers, but is inefficient for Diffusion models due to large activations overhead; and sequence parallelism [26], [27], which divides input tokens across GPUs and is conceptually equivalent to patch parallelism [12] for Diffusions as they both split a single request’s input across devices. These methods are inspiring to this work, but they *exploit parallelism in the spatial dimension solely, thereby overlooking the temporal dynamics, the most key characteristic of diffusion model inference.*

Therefore, we introduce Spatio-Temporal Adaptive Diffusion Inference (*STADI*), the first diffusion-tailored inference framework that directly leverages iterative steps, the fundamental building blocks of each inference request, to mitigate GPU idle periods arising from system heterogeneity, complemented by patch parallelism as a supplementary strategy.

This dual-dimensional method effectively minimizes inference latency while preserving image generation quality. To achieve this, *STADI* makes the following technical contributions.

- **First implementation of heterogeneity-aware distributed diffusion model inference framework:** To the best of our knowledge, this is the first work that investigates how state-of-the-art diffusion models can be distributed and accelerated under *system heterogeneity*. We deploy SDXL [3], one of the most representative diffusion models, for image generation, and implement adaptive patch parallelism and step-specific model synchronization on multi-GPU systems with diverse computational capabilities across devices. Experiments demonstrate that *STADI* can reduce inference latency by 27.01% – 45.36%.
- **First fine-grained step and patch parallelism strategy.** We are the first to propose a spatio-temporal adaptive parallelism mechanism optimizing both step and patch size across devices. 1) Temporally, *STADI* decouples denoising trajectories across devices by assigning different denoising steps after shared warmup phases, according to profiled GPU speeds and a least-common-multiple-minimizing quantization strategy. It preserves fidelity while reducing desynchronization and idle time. 2) Spatially, it employs elastic patch size mending, scaling partitioned sub-regions to balance compute load. This dual-axes adaptation fundamentally replaces static patch parallelism with a more flexible parallel approach, ensuring state consistency across uneven devices.
- **Theoretical Guarantee:** To facilitate analysis, we investigate an advanced diffusion inference framework, DDIM [28] (detailed in Section II-A), which reduces DDPM’s inference steps by a pre-determined factor. We provide a theoretical error bound on the predicted output, which is not covered in the original DDIM work. We then show that *STADI* maintains the same order of error bound as DistriFusion. While DistriFusion operates in homogeneous multi-GPU systems, *STADI* can serve heterogeneous multi-GPU systems.

## II. BACKGROUND AND RELATED WORK

### A. Diffusion Model and Inference Acceleration

Standard diffusion model inference paradigm, which is centered at a gradual denoising process to synthesize data [1]. The training phase comprises two processes: for each step, a *forward process* corrupts an input image  $x_0$  with a Gaussian noise for any randomly sampled timestep index  $t$  to produce a noisy output  $x_t$ , followed by a *reverse process* that takes  $x_t$  as input to the neural network (e.g., U-Net [29]) to generate a noise (prediction) for a randomly sampled step  $t \in \{1, \dots, T\}$ . The model learns to recover Gaussian noise (ground truth) by gradient-based training. Differently, inference, which our work focuses, does not have forward processes. As shown in Figure 1, we start from a Gaussian noise  $\tilde{x}_T$  and iteratively take each  $\tilde{x}_t$  as input of the U-Net and generate  $\tilde{x}_{t-1}$ , and so on, a.k.a. denoising back to the target distribution over a

number of steps. Formally, the forward process and reverse process are defined as follows.

**Forward process.** The forward process of DDPM [1] is a Markov chain that gradually adds Gaussian noise to data over  $T$  steps, transforming structured data into pure noise.

$$q(x_t|x_0) = \mathcal{N}(x_t|\alpha_t x_0, \sigma_t^2 \mathbf{I}), \quad (1)$$

where  $\alpha_t, \sigma_t$  control the noise schedule and both are differentiable for  $t$ .

**Reverse process.** The reverse process learns to denoise data using a neural network  $\epsilon_\theta$  (U-Net [29] or DiTs [4]). It approximates:

$$p_\theta(x_{t-1}|x_t) = \mathcal{N}(x_{t-1}; \mu_\theta(x_t, t), \Sigma_\theta(x_t, t)), \quad (2)$$

**Diffusion inference acceleration.** Latent diffusion models [2] improve efficiency by denoising in a compressed latent space, enabling prompt-guided high-resolution generation. While the complexity of diffusion is reduced from the pixel space of the original image to the latent space, the computational overhead of executing thousands of steps still remains a prohibitive problem. To mitigate this, many sampling acceleration strategies have emerged: DDIM [28] reformulates the reverse process as a deterministic ordinary differential equations (ODEs) [30], [31], enabling significant step reduction while preserving image quality. Lu et al. [31], [32] identified the semi-linear structure of diffusion ODEs and devised higher-order solvers. Moreover, while significant research focuses on optimizing solvers for diffusion SDEs [1], [32]–[35], ODE-based solvers remain the preferred choice.

As illustrated in Figure 4, the first-order solver [31] proposed the following definition showing that  $T$  steps corresponding to those in DDPM can be grouped into  $M$  blocks, each of which consists of  $\frac{T}{M}$  steps, and then the predicted noisy sample  $\tilde{x}_{t_m}$  can be computed as follows

**Lemma 1** (DPM-Solver-1 [31], DDIM). *Given  $x_T$  and  $M+1$  steps  $\{t_m\}_{m=0}^M$  decreasing from  $t_0 = T$  to  $t_M = 0$ . Then the sequence  $\{\tilde{x}_{t_m}\}_{m=1}^M$  is computed as follows:*

$$\tilde{x}_{t_m} = \frac{\alpha_{t_m}}{\alpha_{t_{m-1}}} \tilde{x}_{t_{m-1}} - \sigma_{t_m} (e^{h_m} - 1) \epsilon_\theta(\tilde{x}_{t_{m-1}}, t_{m-1}), \quad (3)$$

where  $h_m = \lambda_{t_m} - \lambda_{t_{m-1}}$ .

**Insight.** This line of work on reducing inference steps offers us the following insight: during multi-GPU parallel inference, we can leverage employ diverse step counts to tackle with the heterogeneity of GPUs. But the challenge is non-trivial, as the inference quality may deteriorate with various denoising steps across distributed inference nodes due to inference results hard to align with each other.

### B. Diffusion Inference Frameworks on Multi-GPU Systems

Existing multi-GPU parallelism for diffusion models primarily focus on spatial partitioning or pipeline optimizations. DistriFusion [12] is an advanced diffusion inference framework that partitions an input noise into uniform patches distributed across GPUs, leveraging patch parallelism to reuse

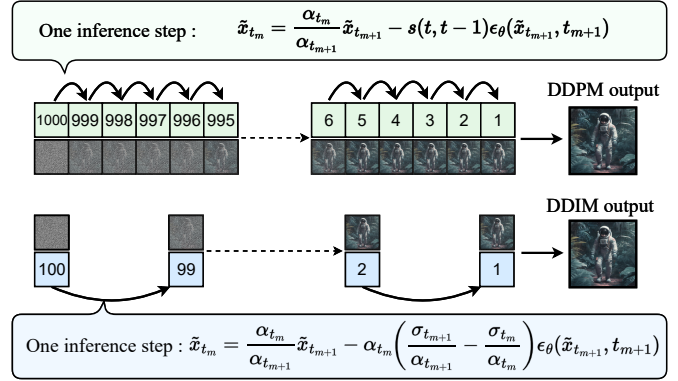


Fig. 4. Architectural comparison between Denoising Diffusion Probabilistic Models (DDPM) and Denoising Diffusion Implicit Models (DDIM).

stale activations from the previous inference step for asynchronous communication. However, its uniform patching strategy assumes power-of-2 GPU numbers and homogeneous GPU capabilities, causing load imbalance when devices exhibit computational disparities. PipeFusion [13] extends this to DiTs [4] via patch-level pipeline parallelism, distributing DiT blocks across devices and reusing stale features to minimize communication. Although memory-efficient for large DiTs, its rigid pipeline stages lack adaptability in computational heterogeneity scenario and rely on static pre-segmentation. Moreover, load imbalance occurs in PipeFusion when the number of transformer layers isn't a multiple of the number of GPUs. Similarly, AsyncDiff [14] pre-divides model layers for pipelined execution, while ParaStep's [15] reuse-then-predict mechanism reduces communication overheads.

Unfortunately, as demonstrated in Figure 2, these frameworks suffer from straggler effects under system heterogeneity. We take a step forward by designing a novel temporal adaptation strategy to mitigate the stragglers' GPU idle time.

### C. Multi-GPU System for Non-Diffusion DL Inference

The escalating computational demands of deep generative models have driven the widespread adoption of multi-GPU systems to accelerate inference [36], [37]. Existing efforts follow two main directions: multi-task throughput maximization, and single-request latency reduction. The first direction focuses on maximizing cluster-wide throughput for concurrent requests. Early systems for homogeneous clusters, such as Clipper [38] and Nexus [39], employed request batching and multi-tenant scheduling. This was later extended to heterogeneous environments by works like AEML [19], which dynamically redistributes workloads based on real-time performance profiling.

This work focuses on accelerating a single inference task, for which prior work explores several parallelism strategies. (1) *Pipeline parallelism* splits models into sequential stages. Systems like PPipe [24] adapt this idea to heterogeneous GPUs by balancing stage sizes and batch allocations; similar

approaches extend to DAG-structured models on edge devices [22], [23]. PASTA [40] extends this technique to vertical federated learning with staleness control, overlapping communication and computation to accelerate training. (2) *Tensor parallelism*, introduced by Megatron-LM [25], partitions weight matrices within layers to enable parallel computation. Extensions like HeteGen [41] adapt this for CPU–GPU hybrid setups to mask memory bottlenecks. (3) *Sequence parallelism* partitions the input data (i.e., the token sequence) across devices. This has become a key technique for handling long contexts in LLMs. State-of-the-art approaches like DeepSpeed-Ulysses [26] use efficient all-to-all collectives, while others like Ring-Attention [27] use P2P communication to compute global attention on partitioned data. Despite their strengths, these approaches primarily exploit spatial parallelism within individual inference steps, as they do not target diffusion models. Our work directly leverages denoising steps, the core component of diffusion inference, and we introduce a novel spatio-temporal adaptation parallelism strategy accordingly, enabling adaptive step reduction and patch resizing across heterogeneous GPUs.

### III. METHOD

#### A. Overview

Existing parallel diffusion inference schemes often perform poorly on heterogeneous or partially utilized multi-GPU systems. Intuition suggests that static partitioning strategies commonly used in homogeneous systems become inefficient bottlenecks for diffusion inference in heterogeneous, potentially busy multi-GPU environments. Therefore, realizing efficient parallelization demands flexible and fine-grained adjustments to each GPU’s temporal computation depth (steps) and spatial computation scope (patch size).

Inspired by DDIM and patch parallelism, therefore, we propose *Spatio-Temporal Adaptive Diffusion Inference (STADI)*, a novel inference acceleration algorithm tailored for diffusion models deployed on heterogeneous multi-GPU systems. The core innovation of *STADI* lies in its dual-axis adaptive scheduling mechanism: (1) *Temporal Adaptation*, which adaptively determines the number of steps  $M_i$  assigned to each GPU  $i$ , and (2) *Spatial Adaptation*, which adaptively allocates a patch  $p_i$  of size  $P_i$  to each GPU  $i$  as a fine-grained complement to the temporal step partitioning.

**Line-by-line Algorithm Interpretation.** The pseudocode in Algorithm 1 outlines *STADI*. It begins with temporal adaptation by computing distinct steps for each GPU, prioritizing larger steps allocations to faster devices to balance processing time (lines 1-3). Subsequently, spatial adaptation determines patch sizes based on each GPU’s effective speed and allocated steps to further equalize workload (lines 4-6). During inference, all GPUs first conduct warmup steps where both buffer and output are gathered synchronously (lines 9-12). The inference loop then operates adaptively: as shown in Figure 5, for faster GPUs, the system alternates between synchronizing to obtain noisy outputs and reusing the noisy output from

---

#### Algorithm 1: *STADI*: Spatio-Temporal Adaptive Diffusion Inference

---

**Input :** An initial noise  $x_{t_0}$ , a pre-trained diffusion model  $\epsilon_\theta(\cdot, \cdot)$ , effective speed of all GPUs  $\{v_i\}_{i=0}^{N-1}$ , a base step number  $M_{\text{base}}$ , and a warmup step number  $M_{\text{warmup}}$

**Output:** The final image  $\tilde{x}_{t_M}$  predicted by *STADI*.

```

1 // Step 1: Temporal Adaption
2 for GPU  $i = 0$  to  $N - 1$  do
3   Get steps  $M_i$  by Equation (4).
4 // Step 2: Spatial Adaption
5 for GPU  $i = 0$  to  $N - 1$  do
6   Get patch size by  $P_i = \frac{v_i/M_i}{\sum_{j=0}^{N-1} v_j/M_j} \cdot P_{\text{total}}$ 
7 // Step 3: Inference Phase
8 for GPU  $i = 0$  to  $N - 1$  in parallel do
9   for  $m^{(i)} = 0$  to  $M_{\text{warmup}} - 1$  do
10    Conduct one-step inference on  $p_i$  with buffer.
11    Update buffer synchronously.
12    Get  $\tilde{x}_{t_m}$  by synchronous All-Gather
13   for  $m^{(i)} = M_{\text{warmup}}$  to  $M_i$  do
14    Conduct one-step inference on  $p_i$  with buffer.
15    if GPU  $i$  is fast then
16      if  $(m^{(i)} - M_{\text{warmup}})\%2 == 0$  then
17        Update buffer asynchronously.
18        Get  $\tilde{x}_{t_m}$  by synchronous All-Gather
19      else
20        No update for buffer.
21        Get  $\tilde{x}_{t_m}$  from last step.
22    else
23      Update buffer by asynchronously.
24      Get  $\tilde{x}_{t_m}$  by synchronous All-Gather
25 Return: Denoised image  $\tilde{x}_{t_M}$ 

```

---

the previous step without synchronization (lines 13-21); meanwhile, slower GPUs consistently perform synchronization after each local computation (lines 22-24). The final denoised image is returned after this process (line 25).

By evaluating both the inherent computational heterogeneity and the current load state across the system prior to inference, *STADI* intelligently allocates computational resources in a load-balanced manner. Figure 5 illustrates the high-level architecture of the *STADI* system, where the adaptive scheduler coordinates heterogeneous GPUs and performs spatio-temporal resource allocation.

#### B. System Model and Problem Formulation

We consider a system comprising  $N$  heterogeneous GPUs, each with a relative computational capability  $c_i > 0$  (the fastest GPU is normalized to  $c_i = 1$ , and slower devices have  $c_i < 1$ ) and a background utilization  $\rho_i \in [0, 1]$  (0 idle, 1 fully loaded). Parameter  $c_i$  can be obtained offline

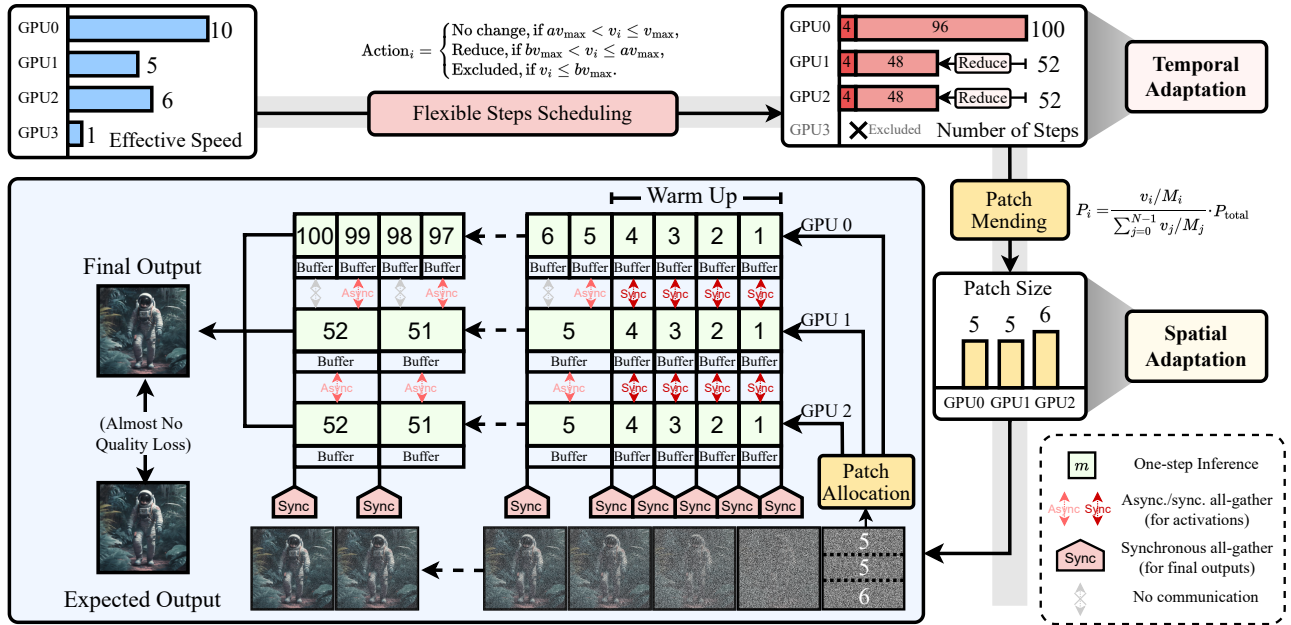


Fig. 5. Overview of *STADI*.

via benchmarking, while  $\rho_i$  is measured via system APIs to capture current workload.

Building on the DDIM sampling process, our method generates images from an initial noise sample through  $M$  denoising steps, where  $M$  governs a tradeoff between generation fidelity and computation latency. To accelerate this process, we adopt the patch parallelism strategy in *DistriFusion* by partitioning the initial noise into spatial patches processed concurrently across multiple GPUs.

Given an initial noise  $x_{i_0}$  and a pre-trained diffusion model  $\epsilon_\theta(\cdot, \cdot)$ , the problem is to find an optimal scheduling strategy, i.e., a set of assignments  $(M_i, P_i)$  for each GPU  $i$  that minimizes the end-to-end generation latency  $R_{\text{total}}$ . Specifically,  $R_{\text{total}}$  is governed by the per-GPU processing latency  $R_i(M_i, P_i, c_i, \rho_i)$ , which is the computation time for GPU  $i$  to complete  $M_i$  steps on patch  $p_i$  under current load  $\rho_i$ .

Our proposed strategy, *STADI*, addresses this optimization problem by creating a joint spatio-temporal workload distribution. Unlike prior methods like *DistriFusion* that employ a uniform temporal assignment, *STADI* innovatively co-adjusts both  $M_i$  and  $P_i$ . By tailoring both the spatial and temporal workload to each GPU's specific capabilities and current load, *STADI* achieves a truly balanced execution.

### C. Temporal Adaptation: Flexible DDIM Steps Scheduling

To mitigate latency from straggler GPUs, our temporal adaptation mechanism adaptively schedules the number of DDIM steps for each GPU. The process begins with a crucial warmup phase, where all GPUs execute a uniform number of steps  $M_{\text{warmup}}$  to ensure model convergence. The core strategy begins with estimating the *effective speed*  $v_i$  for each GPU based on  $c_i$  and  $\rho_i$ . We identify the fastest GPU with speed

$v_{\text{max}}$  and assign it a base step number  $M_{\text{base}}$ . We then assign each  $M_i$  according to the following formulation:

$$M_i = \begin{cases} M_{\text{base}} & \text{if } av_{\text{max}} < v_i \leq v_{\text{max}}, \\ \frac{1}{2} M_{\text{base}} + \frac{1}{2} M_{\text{warmup}} & \text{if } bv_{\text{max}} < v_i \leq av_{\text{max}}, \\ \text{(Excluded)} & \text{if } v_i \leq bv_{\text{max}}, \end{cases} \quad (4)$$

where  $0 < b < a < 1$  are the hyperparameters, representing a trade-off between latency and quality; our practical choices for them will be illustrated in Section V. This strategy halves the computation steps for slower GPUs, allowing them to complete their tasks faster. Basically, it minimizes the lowest common multiple of inference step sizes across multiple GPUs, thereby preventing generation quality degradation due to extended communication intervals. To avoid severe performance degradation, the extremely slow GPUs ( $v_i < bv_{\text{max}}$ ) are excluded. This adaptive scheduling effectively balances the computation load, minimizing per-interval bottlenecks and significantly reducing overall latency.

### D. Spatial Adaptation: Fine-grained Patch Size Mending

Temporal Adaptation alone leaves a residual workload imbalance, as all GPUs still process patches of uniform size. Our spatial adaptation method, *Patch Size Mending*, resolves this by allocating patch sizes  $P_i$  proportional to each GPU's effective processing rate, defined as  $\frac{v_i}{M_i}$  to account for both its speed  $v_i$  and assigned steps  $M_i$ .

To balance the computational load, we equalize the effective computational rate  $\frac{v_i/M_i}{P_i}$  across all GPUs, subject to the spatial coverage constraint  $\sum P_i = 1$ . This yields the optimal patch size for each GPU  $i$ :

$$\frac{v_0/M_0}{P_0} = \frac{v_1/M_1}{P_1} = \dots = \frac{v_{N-1}/M_{N-1}}{P_{N-1}},$$

$$P_i = \frac{v_i/M_i}{\sum_{j=0}^{N-1} v_j/M_j} \cdot P_{\text{total}}, \quad (5)$$

where  $P_{\text{total}}$  is the spatial size of the full image. This formulation mends the residual imbalance from Temporal Adaptation. Consequently, all GPUs finish processing within similar latency per synchronization interval. In practice,  $P_{\text{total}}$  must also satisfy hardware/operator constraints (e.g., power-of-two dimensions) – these implementation nuances are explained in our experimental configuration.

In summary, *STADI* achieves a twofold latency reduction: 1) Temporal Adaptation frees up more computing resources on slower GPUs and reduces the coarse-grained workload at the same time, avoiding them from becoming bottlenecks. 2) Spatial Adaptation then fine-tunes this by reallocating spatial data, maximizing the collective utilization of all available compute resources.

#### IV. THEORETICAL ANALYSIS

##### A. Temporal redundancy in *DistriFusion*

The concept of *temporal redundancy* was first proposed by Pipefusion [13], who formalized the phenomenon observed in *DistriFusion* [12] – the small gap between inputs and activations across consecutive diffusion timesteps, which can be defined as  $|\Delta\tilde{x}_{t_m}| = |\tilde{x}_{t_m} - \tilde{x}_{t_{m+1}}|$ . Such temporal redundancy enables the potential for parallelizing inference.

In this subsection, we will quantitatively analyze the temporal redundancy present in first-order solvers such as DDIM.

**Theorem 1** (Upper bound of temporal redundancy in *DistriFusion*). *Under the assumptions of bounded states, model outputs, and smooth diffusion parameters, the single-step difference in the DDIM update satisfies:*

$$|\tilde{x}_{t_m} - \tilde{x}_{t_{m+1}}| \leq \frac{CT}{M} = \mathcal{O}\left(\frac{1}{M}\right), \quad (6)$$

where  $C = KB + \sigma_{\max}C_eE$  is a constant independent of  $M$  and  $m$ . We denote  $\tilde{x}_{t_m}^{(i)}$  as the output of the  $i$ -th GPU at step  $t_m$ . Since multiple GPUs share identical inference steps, the results after each synchronization are semantically aligned. This yields  $|\tilde{x}_{t_m}^{(i)} - \tilde{x}_{t_{m+1}}^{(j)}| = |\tilde{x}_{t_m} - \tilde{x}_{t_{m+1}}|$  for any devices  $i$  and  $j$ , hence Equation (6) represents the upper bound of temporal redundancy in *DistriFusion*.

*Proof.* See appendix.  $\square$

Theorem 1 analyzes the asymptotic behavior of the upper bound on  $|\Delta\tilde{x}_{t_m}|$  as  $M$  increases. Empirical experiments by *DistriFusion* demonstrate that such redundancy with upper bound  $\mathcal{O}(1/M)$  that does not impact output quality, which is proven to converge in patch parallelism and exploited to accelerate inference in the multi-GPU system.

##### B. Temporal redundancy in *STADI*

The preceding section established that temporal redundancy in *DistriFusion* is bounded by  $\mathcal{O}(1/M)$ , allowing computation-communication overlap across GPUs. We will now extend this

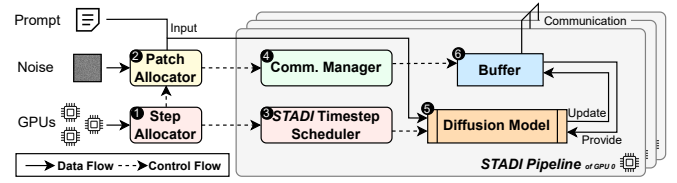


Fig. 6. System architecture.

theorem to analyze the temporal redundancy of *STADI* when the inference steps on each GPU are not consistent.

**Theorem 2** (Upper bound of temporal redundancy in *STADI*). *Under the assumptions of bounded states, model outputs, and smooth diffusion parameters, for two devices  $i$  and  $j$  whose step count satisfies  $nM_i = M_j = M$ , the step difference of their activation satisfies:*

$$\left| \tilde{x}_{t_m}^{(i)} - \tilde{x}_{t_{m+n}}^{(j)} \right| \leq \mathcal{O}\left(\frac{1}{M}\right), \quad (7)$$

where  $t_m^i = t_m^j = s$  and  $t_{m+1}^i = t_{m+n}^j = t$ .

*Proof.* See appendix.  $\square$

Theorem 2 characterizes the upper bound of temporal redundancy using different DDIM schedulers, with a order consistent with using homogeneous DDIM schedulers in Theorem 1. This implies a significant capability: Even when DDIM schedulers operate with *dissimilar step counts*, we can still achieve convergence of the inference process across multiple GPUs by employing appropriate communication operations to align activation information. This enables load balancing by assigning fewer steps to slower GPUs, freeing their computational resources at a minimal cost to quality.

#### V. EVALUATION

This section details our experimental methodology and results. We first introduce the experimental setup, including dataset, models, and baselines. We then present a comprehensive performance analysis of our algorithm under various configurations, followed by ablation studies to validate the effectiveness of its individual components.

##### A. Experimental Settings

**Hardware Configuration & Software Environment.** Experiments were performed on a cluster equipped with two RTX 4090 GPUs interconnected via PCIe, as detailed in Table I. The cluster deployed Python 3.10, PyTorch 2.6.0, and NCCL 2.21.5 communication backend. The `diffusers` library serves as the foundation with custom modifications for distributed scheduling.

**Diffusion Model.** We employ Stable Diffusion XL (SDXL) [3], a 2.3B-parameter model, for two primary reasons: (1) its state-of-the-art, high-resolution image generation quality is representative of demanding real-world applications; and (2) its architecture, featuring a mix of convolutions and attention layers, is characteristic of modern large-scale diffusion models.

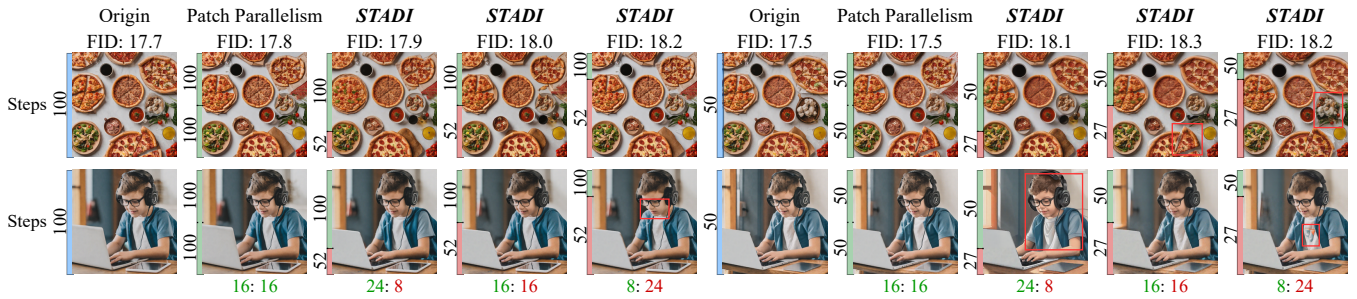


Fig. 7. Image quality visualization on various patch size for step reduction. The FID values are compared with ground truth images. Patch size in red (green) means the steps are (not) reduced.

#Specification	Value	#Specification	Value
GPU type	RTX 4090	CUDA Version	12.4
GPU number	2	Pytorch Version	2.6.0
VRAM Capacity	24GB	cuDNN Version	9.1.0
Tensor Cores	128	NCCL Version	2.21.5

TABLE I: Specifications of the GPU cluster.

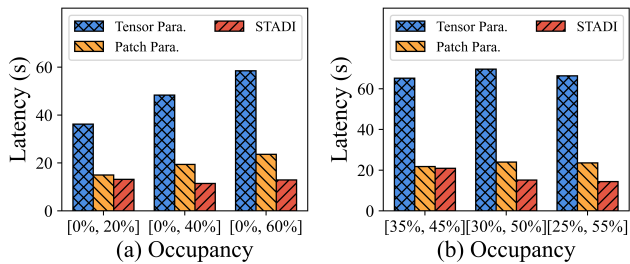


Fig. 8. Latency comparison.

**Baselines.** Comparative evaluation includes two state-of-the-art distributed inference paradigms: patch parallelism from DistriFusion [12] and tensor parallelism. Tensor parallelism achieves distributed diffusion inference by performing synchronous all-reduce at each layer of computation. To ensure a fair comparison, all baselines were re-implemented using identical NCCL communication primitives.

**Evaluation Metrics.** Performance is quantified through end-to-end latency and speedup ratio. Image quality is assessed via the Peak Signal Noise Ratio (PSNR), LPIPS, and Fréchet Inception Distance (FID) on the COCO Captions 2014 validation set [42]. We use partial captions to generate images. PSNR measures pixel-level accuracy between two images. LPIPS measures the perceptual similarity. FID compares sets of generated and real images using a pretrained model to evaluate overall quality and semantic similarity.

**Occupancy Simulation.** To simulate heterogeneous computing power, we run a compute-intensive occupancy program on a target GPU prior to inference. The program adjusts tensor size to stabilize utilization at a preset level, after which the tensor size remains fixed. The ‘‘Occupancy’’ values in the figures thus denote pre-inference workload levels, quantifying

heterogeneous capabilities, consistent with that in Figure 2. **System Architecture.** Figure 6 illustrates the system architecture of the proposed *STADI* Pipeline system. The diagram delineates the processing sequence from inputs (prompt and noise) through core modules (e.g., Patch Allocator, Timestep Scheduler, Communication Manager) to output generation via the Diffusion Model. The arrows explicitly trace the data flow and control flow executed on one GPU.

**Implementation Details.** For a fair comparison, no other acceleration techniques (e.g., batch splitting, CUDA graphs) are applied to the patch parallelism. Regarding the number of inference steps, unless otherwise specified or in experiments involving image quality considerations, we set  $M_{\text{base}} = 100$  and  $M_{\text{warmup}} = 4$ . To satisfy computational constraints of certain operators’ inputs, we set  $P_{\text{total}} = 32$ . The parameters  $a$  and  $b$  control the thresholds for temporal adaptation and GPU usage, respectively. Unless otherwise specified, we set these values to  $a = 0.75$  and  $b = 0.25$ . The effective speed  $v_i$  for each GPU is derived directly from historical inference time profiles. Values reported are averaged over five runs.

**All-Gather for uneven sized tensors.** It is worth mentioning that uneven patch sizes require customized communication. Early versions of `torch` lacked an all-gather implementation adapted for uneven sized tensors. While `all_gather_object` inherently requires a synchronous communication to keep data types and sizes consistent from other devices, it cannot satisfy our asynchronous communication requirements. To address it, we have also developed two asynchronous communication approaches: one achieves this by padding tensors to uniform sizes before performing `all_gather`, while the other uses multiple asynchronous broadcast to emulate `all_gather`. Both two approaches can still mask communication latency within computation.

## B. Main Results

**Latency.** We benchmark *STADI* against baselines for latency in generating  $1024 \times 1024$  images on a 2-GPU system under increasing resource heterogeneity. The first scenario set GPU occupancies to  $[0\%, 20\%]$ ,  $[0\%, 40\%]$ , and  $[0\%, 60\%]$ , keep total resources decreasing. The second set occupancies to  $[35\%, 45\%]$ ,  $[30\%, 50\%]$ , and  $[25\%, 55\%]$ , maintaining total resources fixed while redistributing asymmetry.

$M_{\text{base}}$	#Method	#Patch Size	PSNR ( $\uparrow$ )		LPIPS ( $\downarrow$ )		FID ( $\downarrow$ )		
			w/ G.T.	w/ Orig.	w/ G.T.	w/ Orig.	w/ G.T.	w/ Orig.	
100	Origin	–	9.52	–	0.794	–	<b>17.7</b>	–	
	Patch Parallelism	16:16	9.52	<b>24.65</b>	0.794	<b>0.143</b>	17.8	<b>0.9</b>	
	<i>STADI</i>		24:8	<b>9.56</b>	23.04	0.795	0.188	17.9	1.2
			16:16	9.52	22.14	0.795	0.210	18.0	1.4
			8:24	9.51	23.04	<b>0.793</b>	0.188	18.2	1.3
50	Origin	–	9.64	–	0.796	–	<b>17.5</b>	–	
	Patch Parallelism	16:16	9.62	<b>24.67</b>	0.797	<b>0.145</b>	<b>17.5</b>	<b>0.9</b>	
	<i>STADI</i>		24:8	<b>9.66</b>	23.32	0.801	0.202	18.1	1.4
			16:16	9.62	22.32	0.799	0.234	18.3	1.9
			8:24	9.61	23.13	<b>0.795</b>	0.217	18.2	2.0

TABLE II: Quality metrics comparison.  $\uparrow/\downarrow$ : Higher/Lower is better. Patch size in red (green) means the steps are (not) reduced.

As shown in Figure 8, *STADI* consistently outperforms both baselines across diverse occupancy settings. Tensor parallelism is the slowest in every setting and is severely affected by workload occupancy. In the first scenario in Figure 8(a), our method achieves latency reductions of 12% to 45% over the patch parallelism. When total occupancy is fixed at 80% but redistributed in Figure 8(b), *STADI* achieves 4% to 39% latency reductions. It is noteworthy that when GPU computational capabilities are different yet comparable, the specific setting of  $a$  in Equation 4 does not trigger the temporal reduction. For example, in the [0%, 20%] and [35%, 45%] cases, load balancing is achieved solely by adjusting the patch size, resulting in less latency reduction.

**Quality.** Our main results are shown in Table II by comparing the performance of three methods with two different base steps. The Origin method performs non distributed inference, and the images it generates are called the original images, while the ground truth images refer to images of COCO validation set. Patch parallelism generally achieves higher PSNR values with original images when compared to *STADI*, as it doesn’t reduce the steps on any patch. *STADI* tends to have slightly lower PSNR with original images but higher values with ground truth images, and moreover, the difference between the FID calculated from ground truth images and other methods is minimal (less than 1). This indicates that although the images generated by *STADI* may have slight differences from other methods, they are not inferior to them in terms of content and semantics. Additionally, scaling the base step number  $M_{\text{base}}$  also compromises the generated image quality, which aligns with our theoretical insights.

We compared the FID values computed with ground truth images and visualized in Figure 7. In our algorithm, output quality is mainly influenced by  $M_{\text{base}}$  and the region applied steps reduction. It can be seen that our method still achieves excellent generation quality, expressing the same semantic information as the original image. However, during the execution of step reduction, there will be slight differences in the final image inevitably. We have highlighted several prominent areas with red boxes. We consider this is normal and acceptable.

#Occ.	<i>STADI</i>			
	None	+SA	+TA	+TA+SA
0%, 20%	14.91s	13.16s $1.13\times$	11.30s $1.32\times$	<b>10.85s</b> $1.37\times$
0%, 40%	19.41s	15.13s $1.28\times$	12.05s $1.61\times$	<b>11.43s</b> $1.70\times$
0%, 60%	23.67s	17.73s $1.34\times$	13.03s $1.82\times$	<b>12.92s</b> $1.83\times$

TABLE III: Ablation study. “+SA” means Spatial Adaption while “+TA” means Temporal Adaption.

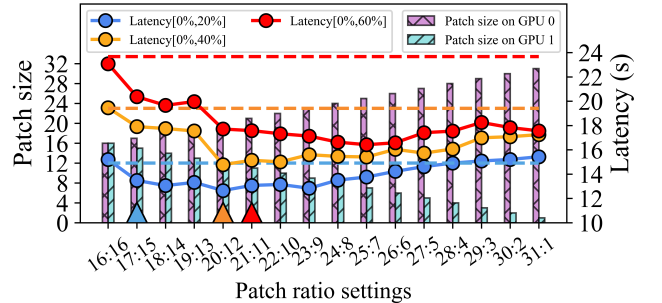


Fig. 9. The inference latency under different workload occupancies and patch sizes. Different colors represent occupancies settings. Dashed lines in corresponding colors indicate pure patch parallelism’s latency under each configuration, while triangles mark the actual patch ratio selected by *STADI*.

### C. Ablation study.

**The impact of patch size.** To isolate and evaluate the efficacy of exclusively utilizing Spatial Adaption (SA) for load balancing under heterogeneous GPU utilization, we disable the Temporal Adaption (TA) to keep uniform steps across GPUs. The sole balancing mechanism is the patch size mending to individual GPUs based on their available computational headroom. As shown in Table III, SA alone improves inference speed by  $1.12\times$ – $1.34\times$  by reducing per-step latency dominated by the slowest GPU. Figure 9 shows how the varying patch ratio impact the latency. When the load gap is too large, patch

allocation based on effective speed may not yield optimal results, as the single-step delay no longer maintains a linear relationship with the patch size due to some fixed overhead.

**The impact of steps reduction.** Temporal Adaption directly addresses the synchronization bottleneck by adaptively halving the inference steps on slower GPUs after the initial warmup phase. As evidenced in Table II, this strategic liberates substantial computational resources on constrained devices, achieving up to 1.82× speedup with [0%, 60%] occupancy. This demonstrates TA’s superior efficacy in mitigating latency induced by severely heterogeneous GPUs. Combining TA+SA yields the lowest latency across all scenarios.

## VI. CONCLUSION

In this work, we presented *STADI*, a novel framework that tackles the latency bottleneck of diffusion model inference on heterogeneous multi-GPU systems. By uniquely exploiting the iterative nature of diffusion sampling, *STADI* introduces fine-grained DDIM step scheduling to free up computational resources on slower GPUs and patch size mending for spatial load balancing. This dual-axes strategy achieves significant latency reductions for SDXL inference without compromising image quality, demonstrating its effectiveness on prevalent heterogeneous hardware. Future work will focus on experiments with large-scale GPU clusters, exploring synergies with techniques like model compression, extending to additional tasks (e.g., video generation), and further optimizations.

## APPENDIX

### A. Proof of Theorem 1

Considering the DDIM update equation (3), the per-step difference is:  $\Delta\tilde{x}_m = \tilde{x}_{t_m} - \tilde{x}_{t_{m-1}}$ . We make the following assumptions:

**Assumption 1.** The inference has a fixed interval  $[t_{\min}, t_{\max}]$  with a step size  $\Delta t_m = t_{m+1} - t_m = T/M$ .

**Assumption 2.** The first derivative of  $\lambda(t) = \log(\alpha_t/\sigma_t)$  is bounded by:  $|\lambda'(t)| \leq L_\lambda$ .

**Assumption 3.**  $\alpha_t \geq \alpha_{\min} > 0, \sigma_t \leq \sigma_{\max}, |\epsilon_\theta(\cdot, \cdot)| \leq E$ , and  $|\tilde{x}_t| \leq B$ .

We then substitute the update equation based on the above assumptions:

$$\Delta\tilde{x}_m = \left( \frac{\alpha_{t_{m+1}}}{\alpha_{t_m}} - 1 \right) \tilde{x}_{t_m} - \sigma_{t_{m+1}}(e^{h_{m+1}} - 1)\epsilon_\theta(\tilde{x}_{t_m}, t_m).$$

For the first term, by Taylor expansion we have:

$$\alpha_{t_{m+1}} = \alpha_{t_m} + \alpha'_t(\tau)\Delta t_m, \text{ for } \tau \in [t_m, t_{m+1}].$$

There, we have:

$$\left| \frac{\alpha_{t_{m+1}}}{\alpha_{t_m}} - 1 \right| = \left| \frac{\alpha'_t(\tau)}{\alpha_{t_m}} \right| \Delta t_m \leq \max_t \underbrace{\left| \frac{\alpha'_t(t)}{\alpha_{t_m}} \right|}_K \Delta t_m,$$

$$\left| \left( \frac{\alpha_{t_{m+1}}}{\alpha_{t_m}} - 1 \right) \tilde{x}_{t_m} \right| \leq KB\Delta t_m.$$

For the second term, since  $h_{m+1} = \lambda_{t_{m+1}} - \lambda_{t_m}$ , we have  $|h_{m+1}| \leq L_\lambda\Delta t_m$ . Further, using  $|e^x - 1| \leq |x|e^{|x|}$ , we have:

$$\begin{aligned} |e^{h_{m+1}} - 1| &\leq |h_{m+1}|e^{|h_{m+1}|} \\ &\leq L_\lambda\Delta t_m \cdot e^{L_\lambda\Delta t_m} \\ &\leq L_\lambda\Delta t_m \cdot e^{L_\lambda T}. \end{aligned}$$

Let  $C_e = L_\lambda e^{L_\lambda T}$ . By  $\sigma_{t_{m+1}} \leq \sigma_{\max}$  and  $|\epsilon_\theta| \leq E$ :

$$|\sigma_{t_{m+1}}(e^{h_{m+1}} - 1)\epsilon_\theta| \leq \sigma_{\max}C_eE\Delta t_m.$$

Finally, by applying the triangle inequality:

$$\begin{aligned} |\Delta\tilde{x}_m| &\leq KB\Delta t_m + \sigma_{\max}C_eE\Delta t_m \\ &= (KB + \sigma_{\max}C_eE)\Delta t_m \\ &= CT/M, \end{aligned}$$

the statement of Theorem VI-A follows.

### B. Proof of Theorem 2

Following the proof of Theorem 3.2 in [31], we have:

$$\tilde{x}_{t_m} = x_{t_m} + \mathcal{O}\left(\frac{1}{M^2}\right) + \mathcal{O}(\tilde{x}_{t_{m-1}} - x_{t_{m-1}}).$$

Then for two DDIM schedulers satisfying  $nM_i = M_j = M$ ,  $\tilde{x}_s^{(i)} = \tilde{x}_s^{(j)} \triangleq \tilde{x}_s$ , and  $x_s^{(i)} = x_s^{(j)} \triangleq x_s$ , we have similar equations below when  $s = t_m^i = t_m^j$  and  $t = t_{m+1}^i = t_{m+1}^j$ :

$$\tilde{x}_t^{(i)} = x_{t_{m+1}^i}^{(i)} + \mathcal{O}\left(\frac{1}{M_i^2}\right) + \mathcal{O}(\tilde{x}_s^{(i)} - x_s^{(i)}),$$

and:

$$\tilde{x}_t^{(j)} = x_{t_{m+1}^j}^{(j)} + \mathcal{O}\left(\frac{1}{M_j^2}\right) + \mathcal{O}(\tilde{x}_{t_{m+1}^j}^{(j)} - x_{t_{m+1}^j}^{(j)}),$$

⋮

$$\tilde{x}_{t_{m+1}^j}^{(j)} = x_{t_{m+1}^j}^{(j)} + \mathcal{O}\left(\frac{1}{M_j^2}\right) + \mathcal{O}(\tilde{x}_s^{(j)} - x_s^{(j)}),$$

Since  $x_{t_{m+1}^j}^{(j)} = x_{t_{m+1}^i}^{(i)} = x_t$ , we have:

$$\begin{aligned} \tilde{x}_t^{(i)} &= x_t + \mathcal{O}\left(\frac{n^2}{M^2}\right) + \mathcal{O}(\tilde{x}_s^{(i)} - x_s), \\ \tilde{x}_t^{(j)} &= x_t + \mathcal{O}\left(\frac{n}{M^2}\right) + \mathcal{O}(\tilde{x}_s^{(j)} - x_s). \end{aligned}$$

Then we can prove that:

$$\left| \tilde{x}_{t_{m+1}^i}^{(i)} - \tilde{x}_{t_{m+1}^j}^{(j)} \right| = \mathcal{O}\left(\frac{n^2}{M^2}\right),$$

Given Theorem 1, we have:

$$\left| \tilde{x}_{t_m^i}^{(i)} - \tilde{x}_{t_{m+1}^j}^{(j)} \right| \leq \mathcal{O}\left(\frac{n}{M}\right).$$

Since  $n$  is much smaller than  $M$ , and using the triangle inequality, we have:

$$\left| \tilde{x}_{t_m^i}^{(i)} - \tilde{x}_{t_{m+1}^j}^{(j)} \right| \leq \mathcal{O}\left(\frac{1}{M}\right).$$

## REFERENCES

- [1] J. Ho, A. Jain, and P. Abbeel, "Denoising diffusion probabilistic models," *Advances in neural information processing systems*, vol. 33, pp. 6840–6851, 2020.
- [2] R. Rombach, A. Blattmann, D. Lorenz, P. Esser, and B. Ommer, "High-resolution image synthesis with latent diffusion models," in *Proceedings of the IEEE/CVF conference on computer vision and pattern recognition*, 2022, pp. 10 684–10 695.
- [3] D. Podell, Z. English, K. Lacey, A. Blattmann, T. Dockhorn, J. Müller, J. Penna, and R. Rombach, "Sdxl: Improving latent diffusion models for high-resolution image synthesis," *arXiv preprint arXiv:2307.01952*, 2023.
- [4] W. Peebles and S. Xie, "Scalable diffusion models with transformers," in *Proceedings of the IEEE/CVF international conference on computer vision*, 2023, pp. 4195–4205.
- [5] J. Ho, T. Salimans, A. Gritsenko, W. Chan, M. Norouzi, and D. J. Fleet, "Video diffusion models," *Advances in neural information processing systems*, vol. 35, pp. 8633–8646, 2022.
- [6] J. Ho, W. Chan, C. Saharia, J. Whang, R. Gao, A. Gritsenko, D. P. Kingma, B. Poole, M. Norouzi, D. J. Fleet *et al.*, "Imagen video: High definition video generation with diffusion models," *arXiv preprint arXiv:2210.02303*, 2022.
- [7] A. Blattmann, T. Dockhorn, S. Kulal, D. Mendelevitch, M. Kilian, D. Lorenz, Y. Levi, Z. English, V. Voleti, A. Letts *et al.*, "Stable video diffusion: Scaling latent video diffusion models to large datasets," *arXiv preprint arXiv:2311.15127*, 2023.
- [8] V. Popov, I. Vovk, V. Gogoryan, T. Sadekova, and M. Kudinov, "Grad-tts: A diffusion probabilistic model for text-to-speech," in *International conference on machine learning*. PMLR, 2021, pp. 8599–8608.
- [9] K. Shen, Z. Ju, X. Tan, Y. Liu, Y. Leng, L. He, T. Qin, S. Zhao, and J. Bian, "Naturalspeech 2: Latent diffusion models are natural and zero-shot speech and singing synthesizers," *arXiv preprint arXiv:2304.09116*, 2023.
- [10] L. Ruan, Y. Ma, H. Yang, H. He, B. Liu, J. Fu, N. J. Yuan, Q. Jin, and B. Guo, "Mm-diffusion: Learning multi-modal diffusion models for joint audio and video generation," in *Proceedings of the IEEE/CVF Conference on Computer Vision and Pattern Recognition*, 2023, pp. 10 219–10 228.
- [11] Z. Tang, Z. Yang, C. Zhu, M. Zeng, and M. Bansal, "Any-to-any generation via composable diffusion," *Advances in Neural Information Processing Systems*, vol. 36, pp. 16 083–16 099, 2023.
- [12] M. Li, T. Cai, J. Cao, Q. Zhang, H. Cai, J. Bai, Y. Jia, K. Li, and S. Han, "Distrifusion: Distributed parallel inference for high-resolution diffusion models," in *Proceedings of the IEEE/CVF Conference on Computer Vision and Pattern Recognition*, 2024, pp. 7183–7193.
- [13] J. Wang, J. Fang, A. Li, and P. Yang, "Pipefusion: Displaced patch pipeline parallelism for inference of diffusion transformer models," *arXiv e-prints*, pp. arXiv–2405, 2024.
- [14] Z. Chen, X. Ma, G. Fang, Z. Tan, and X. Wang, "Asyncdiff: Parallelizing diffusion models by asynchronous denoising," *arXiv preprint arXiv:2406.06911*, 2024.
- [15] K. Wang, B. Li, K. Yu, M. Guo, and J. Zhao, "Communication-efficient diffusion denoising parallelization via reuse-then-predict mechanism," *arXiv e-prints*, pp. arXiv–2505, 2025.
- [16] J. Fang, J. Pan, X. Sun, A. Li, and J. Wang, "xdit: an inference engine for diffusion transformers (dits) with massive parallelism," *arXiv preprint arXiv:2411.01738*, 2024.
- [17] A. Shih, S. Belkhal, S. Ermon, D. Sadigh, and N. Anari, "Parallel sampling of diffusion models," *Advances in Neural Information Processing Systems*, vol. 36, pp. 4263–4276, 2023.
- [18] S. Choi, S. Lee, Y. Kim, J. Park, Y. Kwon, and J. Huh, "Serving heterogeneous machine learning models on {Multi-GPU} servers with {Spatio-Temporal} sharing," in *2022 USENIX Annual Technical Conference (USENIX ATC 22)*, 2022, pp. 199–216.
- [19] Z. Tang, L. Du, X. Zhang, L. Yang, and K. Li, "Aeml: An acceleration engine for multi-gpu load-balancing in distributed heterogeneous environment," *IEEE Transactions on Computers*, vol. 71, no. 6, pp. 1344–1357, 2021.
- [20] S. Zhang, L. Diao, C. Wu, Z. Cao, S. Wang, and W. Lin, "Hap: Spmd dnn training on heterogeneous gpu clusters with automated program synthesis," in *Proceedings of the Nineteenth European Conference on Computer Systems*, 2024, pp. 524–541.
- [21] X. Zhang, "Mixtran: an efficient and fair scheduler for mixed deep learning workloads in heterogeneous gpu environments," *Cluster Computing*, vol. 27, no. 3, pp. 2775–2784, 2024.
- [22] T. Mohammed, C. Joe-Wong, R. Babbar, and M. Di Francesco, "Distributed inference acceleration with adaptive dnn partitioning and offloading," in *IEEE INFOCOM 2020-IEEE conference on computer communications*. IEEE, 2020, pp. 854–863.
- [23] C. Hu and B. Li, "Distributed inference with deep learning models across heterogeneous edge devices," in *IEEE INFOCOM 2022-IEEE Conference on Computer Communications*. IEEE, 2022, pp. 330–339.
- [24] Z. J. Kong, Q. Xu, and Y. C. Hu, "{PPipe}: Efficient video analytics serving on heterogeneous {GPU} clusters via {Pool-Based} pipeline parallelism," in *2025 USENIX Annual Technical Conference (USENIX ATC 25)*, 2025, pp. 679–698.
- [25] M. Shoeybi, M. Patwary, R. Puri, P. LeGresley, J. Casper, and B. Catanzaro, "Megatron-lm: Training multi-billion parameter language models using model parallelism," *arXiv preprint arXiv:1909.08053*, 2019.
- [26] S. A. Jacobs, M. Tanaka, C. Zhang, M. Zhang, S. L. Song, S. Rajbhandari, and Y. He, "DeepSpeed Ulysses: System optimizations for enabling training of extreme long sequence transformer models," *arXiv preprint arXiv:2309.14509*, 2023.
- [27] J. Fang and S. Zhao, "Usp: A unified sequence parallelism approach for long context generative ai," *arXiv preprint arXiv:2405.07719*, 2024.
- [28] J. Song, C. Meng, and S. Ermon, "Denoising diffusion implicit models," *arXiv preprint arXiv:2010.02502*, 2020.
- [29] O. Ronneberger, P. Fischer, and T. Brox, "U-net: Convolutional networks for biomedical image segmentation," in *International Conference on Medical image computing and computer-assisted intervention*. Springer, 2015, pp. 234–241.
- [30] D. Kingma, T. Salimans, B. Poole, and J. Ho, "Variational diffusion models," *Advances in neural information processing systems*, vol. 34, pp. 21 696–21 707, 2021.
- [31] C. Lu, Y. Zhou, F. Bao, J. Chen, C. Li, and J. Zhu, "Dpm-solver: A fast ode solver for diffusion probabilistic model sampling in around 10 steps," *Advances in Neural Information Processing Systems*, vol. 35, pp. 5775–5787, 2022.
- [32] —, "Dpm-solver++: Fast solver for guided sampling of diffusion probabilistic models," *arXiv preprint arXiv:2211.01095*, 2022.
- [33] Y. Song, J. Sohl-Dickstein, D. P. Kingma, A. Kumar, S. Ermon, and B. Poole, "Score-based generative modeling through stochastic differential equations," *arXiv preprint arXiv:2011.13456*, 2020.
- [34] S. Xue, M. Yi, W. Luo, S. Zhang, J. Sun, Z. Li, and Z.-M. Ma, "Sa-solver: Stochastic adams solver for fast sampling of diffusion models," *Advances in Neural Information Processing Systems*, vol. 36, pp. 77 632–77 674, 2023.
- [35] F. Bao, C. Li, J. Zhu, and B. Zhang, "Analytic-dpm: an analytic estimate of the optimal reverse variance in diffusion probabilistic models," *arXiv preprint arXiv:2201.06503*, 2022.
- [36] J. Zhong, Y. Li, S. Liu, J. Duan, X. Zhang, and X. Chen, "Poster: In-network model inference for distributed systems via programmable switches," in *Proceedings of the ACM SIGCOMM 2024 Conference: Posters and Demos*, 2024, pp. 75–77.
- [37] S. Huang, Y. Li, L. Chen, X. Zhang, S. Liu, J. Duan, W. Wu, and X. Chen, "Alleviating all-to-all communication for deep learning recommendation model inference," in *Workshop Proceedings of the 53rd International Conference on Parallel Processing*, 2024, pp. 104–105.
- [38] D. Crankshaw, X. Wang, G. Zhou, M. J. Franklin, J. E. Gonzalez, and I. Stoica, "Clipper: A {Low-Latency} online prediction serving system," in *14th USENIX Symposium on Networked Systems Design and Implementation (NSDI 17)*, 2017, pp. 613–627.
- [39] H. Shen, L. Chen, Y. Jin, L. Zhao, B. Kong, M. Philipose, A. Krishnamurthy, and R. Sundaram, "Nexus: A gpu cluster engine for accelerating dnn-based video analysis," in *Proceedings of the 27th ACM Symposium on Operating Systems Principles*, 2019, pp. 322–337.
- [40] T. Wu, W. Liu, H. Liang, Z. Zhan, J. Duan, C. Wu, J. Zuo, X. Chen, and X. Zhang, "Pasta: Training acceleration for vertical federated learning via adaptive pipeline parallelism," in *2025 IEEE/ACM 33rd International Symposium on Quality of Service (IWQoS)*. IEEE, 2025.
- [41] X. Zhao, B. Jia, H. Zhou, Z. Liu, S. Cheng, and Y. You, "Hetegen: Heterogeneous parallel inference for large language models on resource-constrained devices," *arXiv preprint arXiv:2403.01164*, 2024.
- [42] X. Chen, H. Fang, T.-Y. Lin, R. Vedantam, S. Gupta, P. Dollár, and C. L. Zitnick, "Microsoft coco captions: Data collection and evaluation server," *arXiv preprint arXiv:1504.00325*, 2015.